Electronic Supplementary Information

High-performance composite separator based on the synergy of vermiculite and laponite for lithium-ion batteries

Peijie Xu[a,b], Xiaoyun Yan[c], Yi Zhou[*a], Chunyuan Wang[d], Hongfei Cheng[*e], Yihe Zhang[*a]

1. Chemicals

VMT and LPT were purchased from Alibaba. N-methyl-2-pyrrolidone (NMP, 99%) and N, N-dimethylformamide (DMF, analytical grade) were supplied by Xilong Scientific Co., Ltd. PVDF (solef 5130, 1.75-1.78 g cm^{-3}) power, conductive carbon black, lithium iron phosphate ($LiFePO_4$) power, discs lithium metal anode (15.8 mm), coin cells (CR2032), and commercial electrolyte (LBC310) were purchased from Saibo Electrochemical Materials Network. Commercial PP membrane was purchased from Celgard (Celgard 2400, USA). Copper foil was supplied by Shengshida Metal Materials Co., Ltd.

2. Battery performance tests

$LiFePO_4$ powder, conductive carbon black, and PVDF were mixed into 4.5 mL of NMP at a mass ratio of 7:2:1 to prepare the cathode material of the battery. The prepared cathode material was spread on the surface of a flat copper foil and then dried at 90°C for 12 h. The payload mass of $LiFePO_4$ is 4-5 mg cm^{-2}. The LBC310 and composite separators with VMT and LPT were used as electrolyte and separator, respectively. A 0.5 mm-thick lithium plate was used as anode. The cathodes (80 μm-thick) and separators were cut into discs (13 mm and 2 cm, respectively) and assemble cells in an Ar-filled glove box.

The liner sweep voltammetry (LSV, between 2.0 and 6.0 V) plots were measured to determine the electrochemical stability of at 1 mV s^{-1} using stainless steel (SS) as corresponding working electrode and lithium plates as the counter electrode, respectively. The electrochemical impedance spectroscopy (EIS) was tested from 0.01 to 100 kHz with an AC amplitude of 5 mV. Both EIS and LSV were performed on an electrochemical workstation (CHI660E). The cyclic voltammetry (CV) and AC

impedance spectroscopy (0.1-250 kHz) were conducted in the same equipment as well. A multichannel Battery Test System (LAND, CT2001A) was applied to conduct the cycling and rate performance.

The ionic conductivity σ (mS cm^{-1}) of testing separators at 25°C was calculated based on equation (1):

$$\sigma = \frac{L}{R \cdot A} \times 1000 \#(1)$$

where R, A, and L are the bulk resistance, the effective test area, and the thickness of testing separators, respectively.

3. Characterizations

X-ray diffraction (XRD) patterns were scanned by an X-ray diffractometer (Bruker D8 advance) with Cu Kα (λ = 0.154 nm) radiation in the 2θ range between 5 and 65° at a speed of 2° min^{-1}. Fourier transform infrared spectroscopy (FTIR) characterization was obtained by a Nicolet IS10 FT-IR spectrometer (32 scans at 4 cm^{-1}) in the region from 4000 cm^{-1} to 400 cm^{-1} at room temperature. The surface morphologies and the thickness of the separators were observed on a HITACHI SU8020 field emission scanning electron microscope (SEM). The nanosheets of VMT and LPT were deposited on copper grids for imaging by employing a JEM 1200EX transmission electron microscope (TEM). The pore size distribution of separators was characterized by an AutoPore IV 9620 mercury injection apparatus. The contact angle of separators was measured by a Dataphysics OCA50 contact angle goniometer.

Soak the dried separators in n-butanol for 2 hours at room temperature, and then calculate the porosity (*P*) of the separators according to equation (2):

$$P = \frac{M_2 - M_1}{\rho V_1} \#(2)$$

where M_1 and M_2 are the dry and wet membrane mass before and after soaking. The ρ and $V_1$are the densities of n-butanol and the volume of the dry separators, respectively.

The electrolyte uptake (φ) was examined by immersing the separators in the liquid electrolyte (LBC310) for 2 h. After removing the excess electrolyte solution on the surface of the membrane, the uptake of electrolyte was calculated using the equation (3),

$$\varphi = \frac{M_2 - M_1}{M_1} \times 100\% \#(3)$$

where M_1andM_2 are the weights of the separators before and after immersing, respectively.

4. Cross-section morphology of the separators

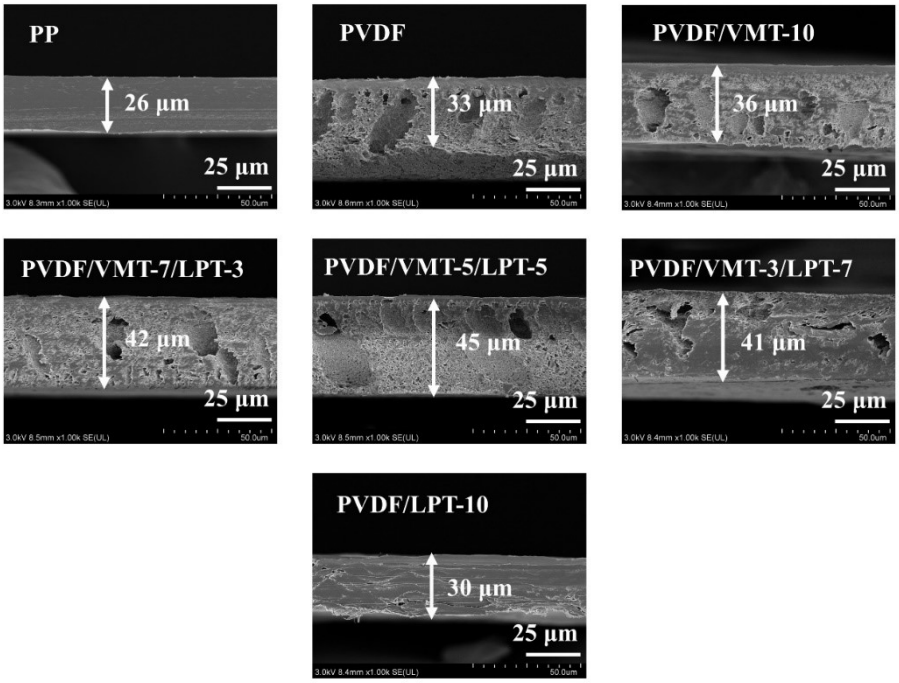

Fig. S1. Cross-sectional SEM images of the different separators.

5. Pore size distribution of the separators

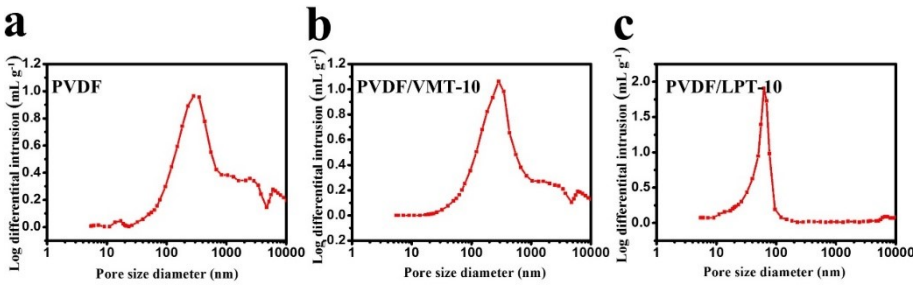

Fig. S2. Pore size distribution of the PVDF, PVDF/VMT-10, and PVDF/LPT-10 by the mercury intrusion method.

6. Wettability of the separators

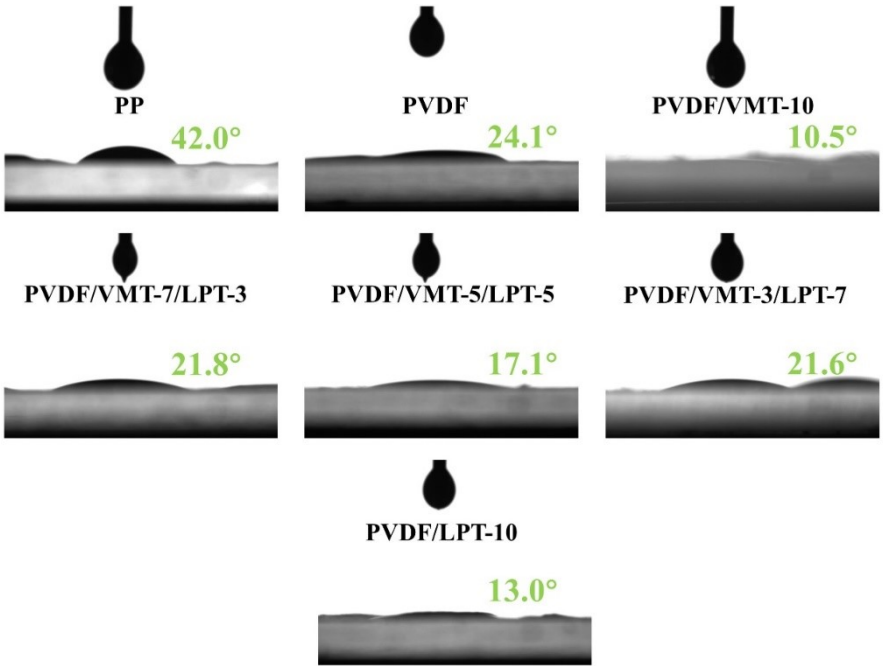

Fig. S3. In situ contact angle measurements of different separators.

7. Structure of the separators

Fig. S4a shows the XRD patterns of VMT, LPT, PVDF, and PVDF/V/L composite separators. The characteristic reflections of VMT (2θ = 8.7 and 26.6°) and LPT (2θ = 6.4, 19.6, 35.1, and 60.9°) can be clearly observed. Two reflections at 2θ = 18.7 and 20.3° can be observed in PVDF pattern indicates a semi-crystalline structure of PVDF [1, 2]. The corresponding reflections of VMT and PVDF are exist in the pattern of PVDF/V/L, and the intensity of VMT reflections decreases with the content decreases. It indicates VMT incorporated into the PVDF matrix and maintain the original structure. However, only the reflection at 6.4° is faintly visible as the content of LPT increases, and other reflections are severely weakened or even disappear. This shows that the crystal structure of LPT collapsed in the PVDF matrix, which is mainly related to the good dispersion of LPT. Moreover, the reflection intensity of PVDF at 2θ = 18.7° is weakened compared with pure PVDF indicates the crystallinity was reduced by the introduction of the inorganic additives, which is beneficial to the conduction of Li^+ [3].

The effect of addition of VMT and LPT was investigated by DSC. As shown in Fig. S4b, the glass transition temperatures of PVDF and PVDF/V/L composite separators are 166.83, 166.17, 166, 165.50, 166.17, and 166.17°C, respectively. It could be shown that the addition of such fillers can decrease the glass transition temperature of the separator system, destroy the crystallinity of the PVDF matrix, and soft the polymer backbone, which has a great promotion effect on the movement of substances in it [4].

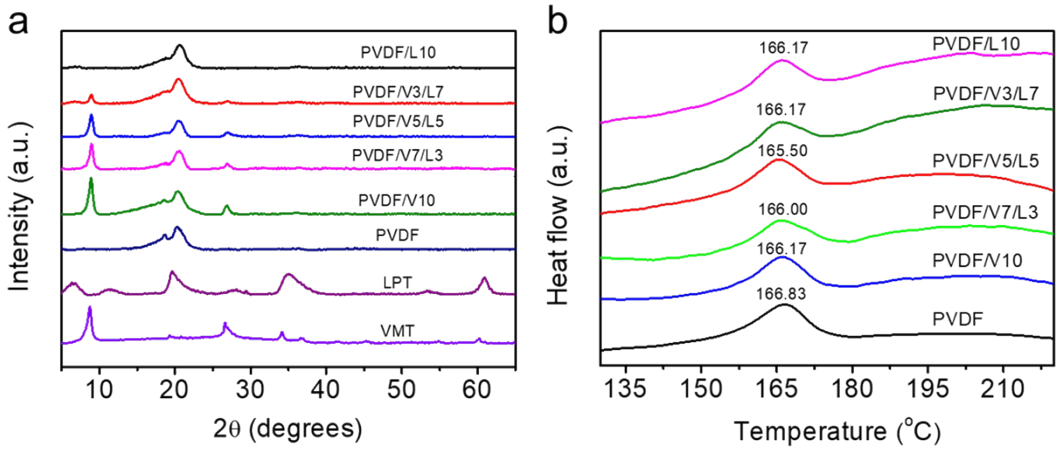

Fig. S4. (a) XRD patterns of VMT, LPT, PVDF, and PVDF/V/L composite separators. (b) DSC curves of PVDF, PVDF/V/L composite separators.

8. Digital photographs of separators

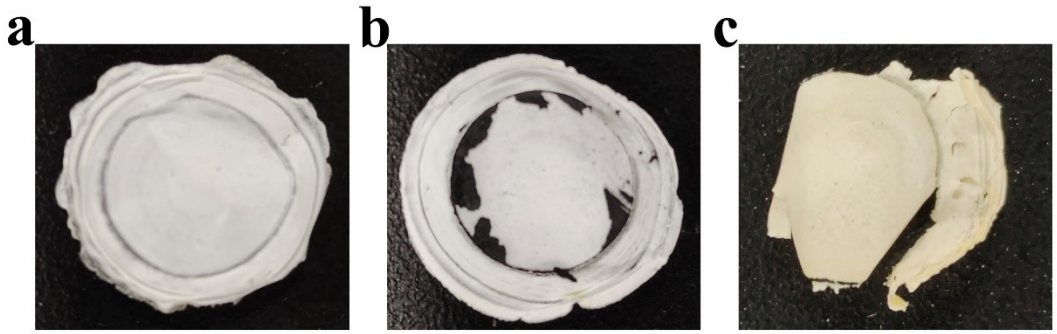

Fig. S5. Digital photographs of PP (a), PVDF (b), and PVDF/V5/L5 (c) after long-term cycles.

9. Thermal shrinkage property

High thermal stability is an indispensable requirement for separators which enables them to preserve their dimension in case of elevated temperatures attributable to short circuit caused by overcharging [5,6]. The snapshots of PP, PVDF, and PVDF/V/L composite separators after exposure at 150°C for 30 min are shown in Fig. S2.

Compared with PP and PVDF/V/L, the degree of thermal shrinkage of PVDF is the most obvious, indicating that the introduction of heat-resistant inorganic nanosheets can successfully reduce the thermal shrinkage of the separators. Interestingly, PVDF/V10 and PVDF/L10 remains substantially original circular shape but PVDF/V5/L5 exhibits a larger deformation. In other words, the separators with only one kind of inorganic additive have a better thermal stability. It can be attributed to the uniform diameter, thickness, and the acidic sites on the surface of vermiculite/laponite nanoparticles provide better thermal oxidation stability to host PVDF matrix [7]. This indicates that the distribution of active sites that react with the organic matrix has a certain effect on the thermal shrinkage performance of the composite separators.

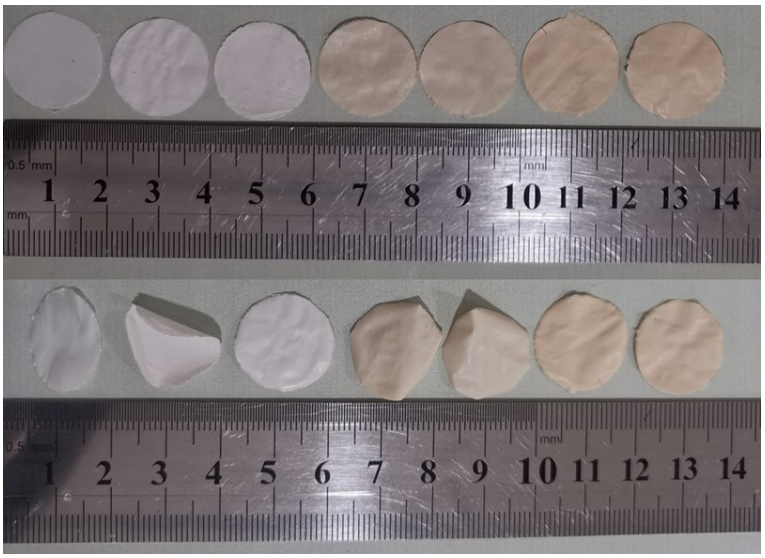

Fig. S6. Snapshots of PP, PVDF, PVDF/L10, PVDF/V3/L7, PVDF/V5/L5, PVDF/V7/L3, and PVDF/V10 after exposure for 30 min at 150°C.

10. Electrolyte resistance ionic conductivity

Tab. S1. Bulk electrolyte resistance R and ionic conductivity at 25°C of different separators.

Membrane	Bulk electrolyte resistance R (Ω)	Ionic conductivity σ (mS cm^{-1})
PP	6.5	0.36
PVDF	7.4	0.32
PVDF/V10	10.6	0.22
PVDF/V7/L3	8.4	0.29
PVDF/V5/L5	3.3	0.72
PVDF/V3/L7	5.8	0.41
PVDF/L10	5.6	0.42

11. Ion conductivity and cycling property comparison

Tab. S2. Ion conductivity and cycling property comparison of this work with recently reported Li-ion batteries with $LiFePO_4$ cathode in the literature.

Separators	Ion conductivity (mS/cm)	Coulombic efficiency (%)	Capacity retention (%)	Life (cycles)	Reference
phenolic resin (AF) modified polyethylene (PE) composite separators	0.604	96.7	86.0	450	[8]
halloysite/polyvinylidene fluoride composite membrane	2.4	/	89.12	100	[3]
Commercial polypropylene (PP) membrane (Celgard 2400)	0.31		84.04	100	[3]
sodium alginate/attapulgite separator	1.15		82.2	700	[5]
Celgard 2325	0.95		68.7	700	[5]
5% PVDF-HFP composite nonwoven separator	0.847		76.8	50	[9]
PVDF/vermiculite/laponite composite separator	0.72	99.5	98.4	100	This work

Reference:

1. R. Miao, B. Liu, Z. Zhu, Y. Liu, J. Li, X. Wang and Q. Li, *Journal of Power Sources*, 2008, **184**, 420-426.
2. H. Yu, Y. Zhang, X. Sun, J. Liu and H. Zhang, *Chemical Engineering Journal*, 2014, **237**, 322-328.
3. H. Xu, D. Li, Y. Liu, Y. Jiang, F. Li and B. Xue, *Journal of Alloys and Compounds*, 2019, **790**, 305-315.
4. M. Wang, F. Zhao, Z. Guo and S. Dong, *Electrochimica Acta*, 2004, **49**, 3595-3602.
5. Q. Song, A. Li, L. Shi, C. Qian, T. G. Feric, Y. Fu, H. Zhang, Z. Li, P. Wang, Z. Li, H. Zhai, X. Wang, M. Dontigny, K. Zaghib, A.-H. Park, K. Myers, X. Chuan and Y. Yang, *Energy Storage Materials*, 2019, **22**, 48-56.
6. X. Hao, J. Zhu, X. Jiang, H. Wu, J. Qiao, W. Sun, Z. Wang and K. Sun, *Nano Letters*, 2016, **16**, 2981-2987.
7. A. K. Solarajan, V. Murugadoss and S. Angaiah, *Scientific Reports*, 2017, **7**, 45390.
8. Q.-Q. Gu, H.-J. Xue, Z.-W. Li, J.-C. Song and Z.-Y. Sun, *Journal of Power Sources*, 2021, **483**, 229155.

9. H. Wang and H. Gao, *Electrochimica Acta*, 2016, **215**, 525-534.